A Highly Accurate Approach That Resolves the Pressure Spike of Elastohydrodynamic Lubrication

E. J. Bissett
D. W. Glander

Mathematics Department,
General Motors Research Laboratories,
Warren, Mich. 48090

We propose an accurate numerical method to solve the classical line contact problem of elastohydrodynamic lubrication. The method incorporates a second order accurate discretization and a straightforward automatic local mesh refinement procedure. Using these elements, we remove discretization errors which have produced significant inaccuracies in previously published results, and we completely resolve the pressure spike which is shown to be smooth on a sufficiently small length scale.

Introduction

The numerical solution of the classical line contact problem of elastohydrodynamic lubrication (EHL) has recently received additional attention [1-6]. In these numerical solutions, one of the most striking features, and one of the most computationally problematic, is the pressure spike.

The pressure spike is a narrow peak of high pressure that occurs toward the downstream end of the pressure profile (see Figs. 1(*a*), 2(*a*), 3(*a*)) between the rolling elements. Little is known about the precise cause of the pressure spike. However, it is known that the spike will not occur when the viscosity is constant, even at high loads [7]. Even the continuity of the derivative of pressure at the top of the spike is subject to controversy, and previous authors who have attempted to use finer meshes to resolve details of the pressure spike have found that the maximum pressure increases with the number of mesh points [5, 6].

We believe that such controversies have arisen from inaccurate numerial results in previous solutions. We remove these inaccuracies with a numerical approach that for the first time completely resolves the pressure spike in even quite difficult cases. In so doing, various techniques are proposed that advance the state-of-the-art in solving the EHL equations generally.

The approach given herein consists of a discretization that has second order errors on a nonuniform mesh. All solution variables, including the unknown exit position, are obtained simultaneously by Newton's method. Following convergence of Newton's method, a local error test is made throughout the solution region, and additional points are inserted where most needed. The current discrete solution, suitably interpolated, is used as an initial guess for Newton's method on the new mesh. The local error test is repeated, followed again by Newton's method until a prescribed error tolerance or a maximum number of mesh points is achieved. Such a technique for dynamically generating converged solutions on a nonuniform mesh is herein reported to completely resolve the gradients in

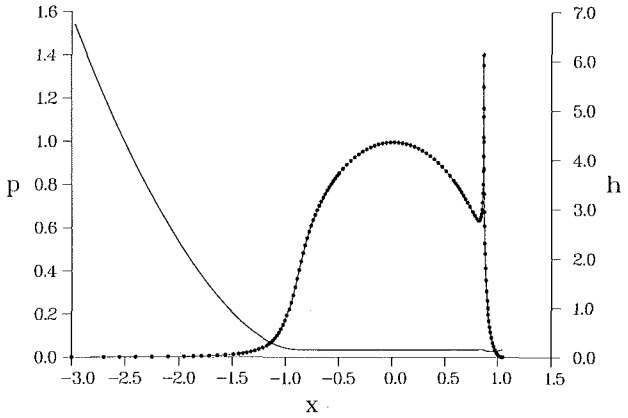

Fig. 1(*a*) $\alpha = 10., \lambda = .04$. Pressure and film thickness over entire interval. Every sixth point is marked on pressure profile.

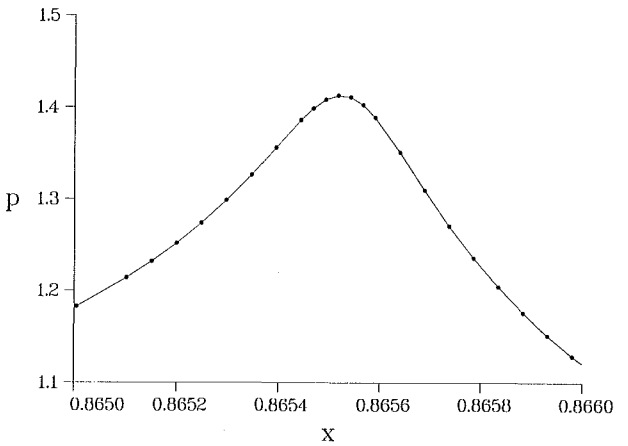

Fig. 1(*b*) $\alpha = 10., \lambda = .04$. Pressure profile near the pressure maximum with every mesh point shown.

Contributed by the Tribology Division of THE AMERICAN SOCIETY OF MECHANICAL ENGINEERING and presented at the ASLE/ASME Tribology Conference, San Antonio, Texas, October 5-8, 1987. Manuscript received by the Tribology Division, January 29, 1987. Paper No. 87-Trib-2.

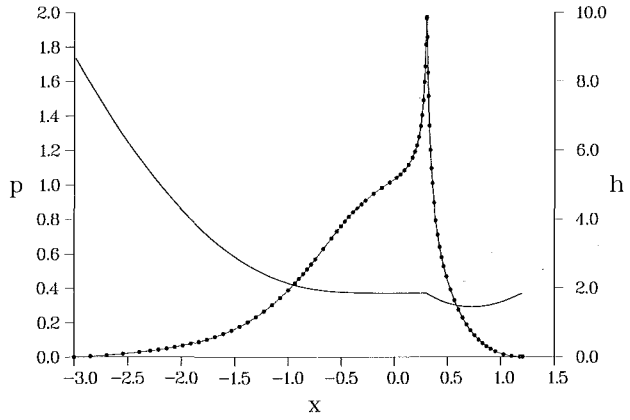

Fig. 2(*a*) $\alpha = 5.046$, $\lambda = 2.96$. Pressure and film thickness over entire interval. Every sixth point is marked on pressure profile. Corresponds to $U = 1 \times 10^{-11}$, $G = 4 \times 10^{3}$, $W = 1 \times 10^{-5}$.

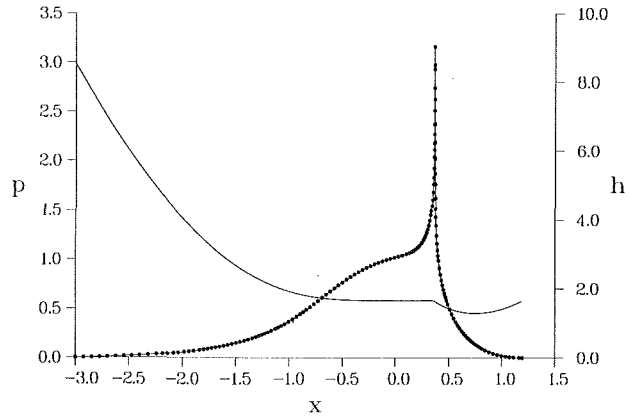

Fig. 3(*a*) $\alpha = 5.352$, $\lambda = 2.339$. Pressure and film thickness over entire interval. Every sixth point is shown on pressure profile. Corresponds to $U = 1 \times 10^{-11}$, $G = 4 \times 10^{3}$, $W = 1.125 \times 10^{-5}$.

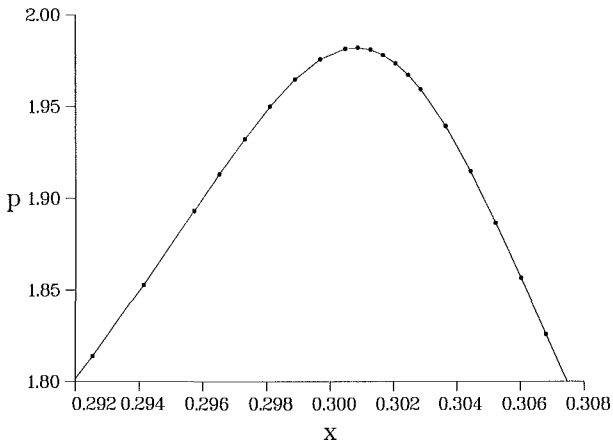

Fig. 2(*b*) $\alpha = 5.046$, $\lambda = 2.96$. Pressure profile near the pressure maximum with every mesh point shown.

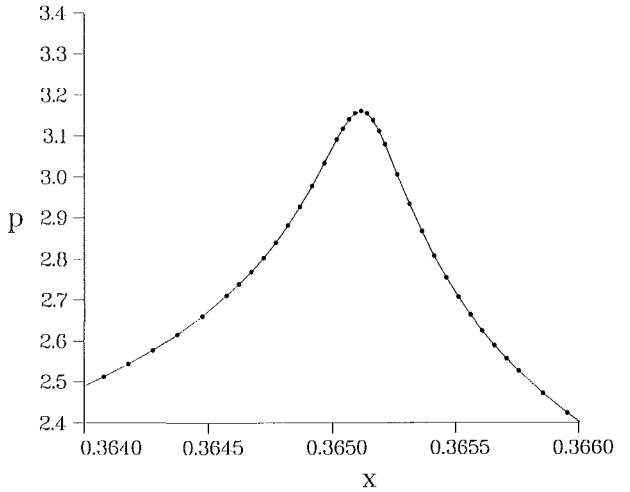

Fig. 3(*b*) $\alpha = 5.352$, $\lambda = 2.339$. Pressure profile near the pressure maximum with every mesh point shown.

the pressure spike. In particular, the spike is shown to have a continuous first derivative when viewed on a suitably small length scale. It is not a singularity.

In the next section, we describe our discrete formulation in detail, and compare it to some of the recent formulations of other authors. Then our automatic mesh refinement procedure is described, followed by a short discussion of the continuation procedure used to generate initial guesses for Newton's method. Results are then presented with particular emphasis on the pressure spike. We close with a discussion of the results.

Discrete Formulation

We begin with the nondimensional equations as given by Kostreva [2], whose notation we modify only for the endpoints, a and b. In particular, we consider the isothermal case of a line contact with pure rolling. The fluid is assumed incompressible, obeying the Barus pressure-viscosity dependence. Only two dimensionless parameters, α and λ, are required to describe the problem for determining the pressure, p, and the film thickness, h.

$$h^3 \frac{dp}{dx} = \lambda e^{\alpha p}[h - h(b)] \tag{1}$$

$$h(x) = x^2 - b^2 + h(b) - \frac{2}{\pi}\int_a^b p(s)\log\left|\frac{x-s}{b-s}\right| ds \tag{2}$$

$$\frac{2}{\pi}\int_a^b p(s)ds = 1 \tag{3}$$

$$p(a) = p(b) = 0 \tag{4}$$

Reynold's equation (1), is used in integrated form, introducing $h(b)$ explicity. The boundary condition $dp/dx(b) = 0$ has been used to obtain equation (1) and is now redundant, since any solution of equation (1) will necessarily satisfy this boundary condition. In the elastic equation, (2), $h(b)$ has also been used to eliminate the more usual composite constant (k in the notation of [2]). Use of the integrated Reynold's equation is highly recommended, since it substantially simplifies the discretization procedure.

In previous work, the location of the free boundary, b, has been problematic. In some approaches, [2] and [6] for example, pressures are cut off below zero and the free boundary is located only to the closest mesh point. In other approaches, [4], and [5] for example, the film thickness is calculated just outside the original interval, [a, b], and interpolated to provide the condition that fixes the free boundary. In the complementarity approach of Kostreva [2], an additional outer loop is devoted solely to establishing the free boundary location. Determination of the free boundary location has been considered sufficiently difficult that Lubrecht [6] considers the problem to be one of the "two severe drawbacks" of the Newton approach.

We avoid all such difficulties with the simple expedient of scaling the problem to a fixed interval before numerical solution. Let

$$z=\frac{x-a}{b-a}, \tag{5}$$

so the computations are now performed on [0, 1] for all b. The parameter b is now an unknown to be determined at the same time and to the same accuracy as the other unknowns of the problem. This change of independent variable introduces some additional nonlinearities into the problem, but they provide no difficulty for the Newton iteration.

The problem on [0,1] becomes the following, after bringing the exponential inside the derivative in Reynold's equation:

$$h^3(z)\frac{d}{dz}[\exp(-\alpha p(z))]=-(b-a)\alpha\lambda[h(z)-h(1)] \tag{6}$$

$$h(z)=(b-a)(z-1)[(a+b)+(b-a)z]+h(1)$$

$$-\frac{2}{\pi}(b-a)\int_0^1 p(s)\log\left|\frac{z-s}{1-s}\right|ds \tag{7}$$

$$\frac{2}{\pi}(b-a)\int_0^1 p(s)ds=1 \tag{8}$$

$$p(0)=p(1)=0 \tag{9}$$

To discretize this system, a nonuniform mesh is introduced: $0=z_0<z_1<\ldots<z_n=1$. Let p_j be the approximation to $p(z_j)$. We want this approximation to have errors no larger than the square of the local mesh spacing. The discrete unknowns are $\{p_j\}_{j=0}^n$, $h(1)$, and b, for a total of $n+3$ unknowns. It is convenient to introduce the half-points, $z_{j-1/2}=(z_{j-1}+z_j)/2$, and $h_{j-1/2}$ which will be a second order approximation to $h(z_{j-1/2})$.

A discrete version of equation (6) written at the half-points results in the first n equations.

$$h_{j-1/2}^3\left[\frac{\exp(-\alpha p_j)-\exp(-\alpha p_{j-1})}{z_j-z_{j-1}}\right]$$

$$+(b-a)\alpha\lambda[h_{j-1/2}-h(1)]=0, \qquad j=1,\ldots,n \tag{10}$$

In this, $h_{j-1/2}$ is obtained from equation (7) written at the half-point. The only approximation required in obtaining $h_{j-1/2}$ is in performing the integration. The integration will have second order errors if p is approximated by its piecewise-linear interpolant in each mesh interval and the resulting integrals are performed exactly. This procedure results in the modified trapezoid rule for the logarithmic kernel of equation (7).

$$\int_0^1 p(s)\log\left|\frac{z_{j-1/2}-s}{1-s}\right|ds\simeq\sum_{i=1}^n a_{ij}p_i+b_{ij}p_{i-1}, \tag{11}$$

where a_{ij} and b_{ij} are given by

$$(z_i-z_{i-1})a_{ij}=-[(s+z_{j-1/2})/2-z_{i-1}](z_{j-1/2}-s)\log|z_{j-1/2}-s|$$

$$+[(s+1)/2-z_{i-1}](1-s)\log(1-s) \tag{12}$$

$$+\frac{1}{2}s(1-z_{j-1/2})\Big|_{s=z_{i-1}}^{s=z_i}$$

$$(z_i-z_{i-1})b_{ij}=[(s+z_{j-1/2})/2-z_i](z_{j-1/2}-s)\log|z_{j-1/2}-s|$$

$$-[(s+1)/2-z_i](1-s)\log(1-s) \tag{13}$$

$$-\frac{1}{2}s(1-z_{j-1/2})\Big|_{s=z_{i-1}}^{s=z_i}$$

Equation (7) yields the result,

$$h_{j-1/2}-h(1)=(b-a)(z_{j-1/2}-1)[(a+b)+(b-a)z_{j-1/2}]$$

$$-\frac{2}{\pi}(b-a)\sum_{i=1}^n a_{ij}p_i+b_{ij}p_{i-1}. \tag{14}$$

This quantity, $h_{j-1/2}-h(1)$, is computed and used internally in the computations rather than $h_{j-1/2}$ to avoid the possible loss of significance in the subtraction of the often nearly-equal quantites, $h_{j-1/2}$ and $h(1)$, in equation (10). When this result is used in equation (10), this equation also contains errors no larger than the square of the mesh spacing.

Three more equations are required to complete the discretization. They are $p_0=0$, $p_n=0$, and the trapezoid rule applied to the load balance, equation (8).

$$\frac{2}{\pi}(b-a)\sum_{i=1}^n\left(\frac{p_{i-1}+p_i}{2}\right)(z_i-z_{i-1})=1 \tag{15}$$

In conclusion, we give $n+3$ equations for the $n+3$ unknowns to be solved by Newton's method. The discretization is second order accurate. We emphasize that no special accomodation of the free boundary location, b, is required in the numerical procedure, and that b is treated simply as another unknown.

Rohde and Oh [8] were the last to use a highly accurate discretization to solve this problem, but their results show only moderate pressure spikes. Most of the other referenced works claim no more than a first order accurate discretization. Kostreva's [2] discretization of Reynold's equation is second order accurate, but only on a uniform mesh and cannot be directly generalized to a nonuniform mesh. Moreover, Kostreva's discrete integration in the elastic equation is not second order accurate even on a uniform mesh. That is, the logarithmic kernel in [2] is discretized simultaneously with the pressure in performing the integration, and the logarithmic kernel does not possess the two bounded derivatives necessary for the trapezoidal rule to be fully second order accurate. Houpert and Hamrock [5] present a second order accurate discretization, but they use a first-order discretization for most of the results they present, stating that it converged more easily.

Mesh Refinement

Automatic mesh refinement is a central component of our approach. Other authors, for example [1] and [5], have used a nonuniform mesh for this problem, but the points are specified a priori. In the approach recommended here, locations of additional mesh points are determined automatically in an outer cycle that continues until a prespecified error tolerance or a maximum number of mesh points is attained. We describe our algorithm in detail below, but other approaches may be equally effective, provided that sufficient care is taken in the presence of the pressure spike. The important point is that each discrete solution should be subjected to some refinement procedure that will insure the insensitivity of the discrete solution to further refinement (that is, convergence under mesh refinement) before one infers properties of the continuous solution from this discrete solution.

The discretization error is controlled by calculating a mesh function, e_j, after each discrete solution. The mesh function, e_j, is related to the discretization error in interval j and will be described in detail below. For now we simply note that we can always arrange for it to be proportional to the local mesh spacing. The actual refinement is carried out by adding one point at a time as follows: (1) the interval with the largest e_j is located, (2) this interval is halved and the pressure at the new mesh point thus created is obtained by linear interpolation, and (3) the error e_j is halved to be shared equally by the two

new subintervals. Points are added in this manner until the worst estimated error is less than the prescribed tolerance or until a prescribed number of new points per refinement step is reached. To insure a degree of regularity to the mesh, additional points are also added so that no mesh interval is more than 2.5 times the size of either neighbor. Once this refinement process is complete, the resulting pressure distribution on all of [0, 1] is resubmitted as an initial guess for Newton's method for the discrete EHL equations. The cycling between refinement and solution is continued until no refinement is necessary to meet the prescribed tolerance or until a maximum number of mesh points is reached (generally, 1000).

This algorithm works to refine the mesh were e_j is largest, with the motivation that it is most efficient to put the new mesh points where they are indeed needed. More formally, we are creating an approximately equidistributing mesh: eventually, all e_j's will be within a factor of 2 using the above algorithm. The use of equidistributing meshes for controlling nonuniform mesh refinement is common in two-point boundary value problems (see [9] and the references therein), and in flame calculations (see [10] and the references therein), for example. It is important to realize that the aim of an equidistributing mesh is to give the best solution possible for the current number of mesh points; it does not guarantee sufficient accuracy of any individual discrete solution. One must still test the discrete solution for insensitivity to further refinement. For the results presented here, we sought insensitivity of pressure maximum value and position when viewed on a length scale sufficiently small to reveal the smoothness of the pressure spike.

Obviously, the success of this approach relies upon an appropriate mesh function, e_j. Common choices use the local truncation error (for example, [9]), or a combination of lower order derivatives of the solution (for example, [10]). When readily available, the local truncation error is the most theoretically sound choice. For our problem, two distinct sources of truncation error can be identified: (1) the truncation error, E_R, associated with the discretization of Reynold's equation, equation (10), when we consider $h_{j-1/2}$ as known exactly, and (2) the truncation error, E_h, associated with the discrete evaluation of $h_{j-1/2}$, equation (14). An immediate problem presents itself in that E_h does not induce a well-defined *local* truncation error. That is, a mesh that would equidistribute the local truncation error for $h_{j-1/2}$ would not necessarily equidistribute the error for the evaluation of $h_{j+10-1/2}$. Nevertheless, our experience has shown that E_h is more important than E_R in obtaining the position and value of the pressure maximum, which is the most challenging part of this calculation. We therefore now focus on how to obtain a mesh function from E_h.

The truncation error of equation (14) arises only from the truncation error of the modified trapezoid rule, equation (11). For a *fixed* $z_{j-1/2}$, we can define a local truncation error, T_{ji}, which represents the contribution to the error over interval i such that

$$\sum_i T_{ji} \propto E_h.$$

A short calculation gives

$$T_{ji} \simeq \frac{1}{12}(z_i - z_{i-1})^3 \left| p''(z_i) \log \left| \frac{z_{j-1/2} - z_i}{1 - z_i} \right| \right| \tag{16}$$

as the dominant term for the local truncation error. Note that it depends nontrivially upon $z_{j-1/2}$, which is why T_{ji} only makes sense as a local truncation error for fixed $z_{j-1/2}$. However, the logarithm has only a weak singularity at two isolated points, $z_i = 1$, and $z_i = z_{j-1/2}$, that is not even strong enough to cancel a single power of $(z_i - z_{i-1})$ at these points. Therefore, if we treat the logarithm as a constant, only a small error is introduced, the dependence upon $z_{j-1/2}$ drops out of T_{ji}, and an approximate local truncation error proportional to $(z_i - z_{i-1})^3 |p''(z_i)|$ can be identified.

Only technical details are required to complete the determination of e_j. To prevent the mesh from becoming too sparse where p'' accidentally vanishes, $|p''|$ is replaced by $|p''| + \gamma |p'|$, since p' is extreme when p'' vanishes ($\gamma = 12$ was used for the examples given below). Finally, a cube root is taken so that e_j will be proportional to the local mesh spacing as mentioned above.

$$e_j = (z_j - z_{j-1})(|p''(z_j)| + \gamma |p'(z_j)|)^{1/3} \tag{17}$$

Crude approximations to these derivatives will suffice.

We close this section with some of our experience in efficiently refining meshes. This computation is dominated by the expense of factoring the Jacobian of the $(n+3)$ nonlinear equations into upper and lower triangular matrices for Newton's method. These full matrices are calculated analytically for each new mesh. Computational efficiency is obtained by seeking the maximum refinement with the minimum of factorizations. Therefore, we iterate with Newton's method using only the first factored Jacobian for up to 50 iterations. If 50 iterations are not sufficient, we back up to the last refinement level and retry the refinement but with only half the number of refining mesh points. Conversely, if Newton's method finds the solution too easily, that is, in 4 iterations or less, the number of points to be added during the next refinement is doubled. These numbers worked well, but we make no claim that they are optimal. The key point is that one can use the information contained in the number of Newton iterates to judge how aggressively to refine on subsequent steps. Generally, the insensitivity of the discrete solutions to mesh refinement grows progressively, so this procedure will allow a steady increase in the number of points added per refinement as the solution is refined.

Obtaining Solutions by Continuation

During the refinement procedure, the initial guess for Newton's method at each step of the refinement is supplied naturally by the solution from the previous refinement step. To supply initial guesses for Newton's method at the beginning of the refinement procedure, that is, on the crudest mesh, a continuation method generates new solutions using nearby, more easily obtained, solutions in the $\lambda - \alpha$ parameter space.

To increase the size of the continuation step from those used in [2], forward Euler steps are used. Specifically, let Y be the $(n+3)$-vector of unknowns, let R be the $(n+3)$-vector of discrete equations for the unknowns to satisfy, and ρ be one of the problem parameters—α, λ or a combination of these two. Having a solution for a particular $\rho = \rho_0$ means

$$R(y(\rho);\rho) = 0 \qquad \text{at } \rho = \rho_0 \tag{18}$$

An approximate solution at a neighboring ρ is available from

$$y(\rho) \simeq y(\rho_0) + (\rho - \rho_0)\frac{dy}{d\rho}(\rho_0). \tag{19}$$

$dy/d\rho(\rho_0)$ is obtained by differentiating (18).

$$\frac{\partial R}{\partial y}\frac{dy}{d\rho} + \frac{\partial R}{\partial \rho} = 0 \quad \text{at } \rho = \rho_0 \tag{20}$$

The $(n+3) \times (n+3)$ matrix, $\partial R/\partial y$, is the Jacobian of the nonlinear system which we have just used to obtain the solution at $\rho = \rho_0$ in equation (18). That is, since the Newton iterations already require the computation of a Jacobian, we use this information twice to permit the simple use of a two-term Taylor series approximation for the new solution in equation (19), rather than a one-term expansion.

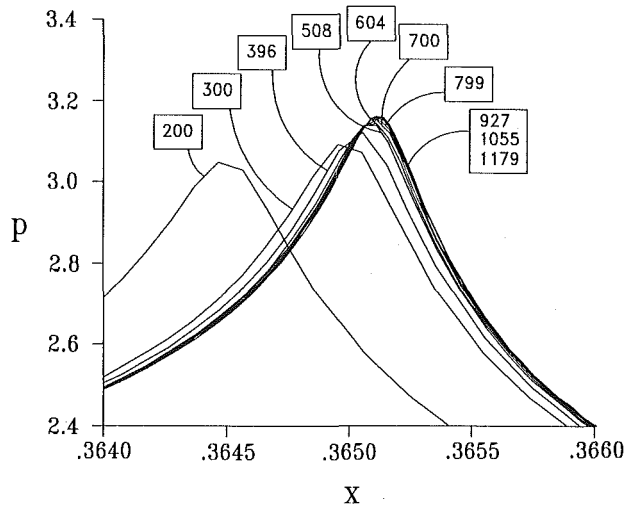

Fig. 4 Discrete pressure profiles near the pressure maximum for the same parameters as Fig. 3. Labels show the number of points used to generate each discrete solution. Above 927 points, the curves are essentially indistinguishable. Mesh point locations surpressed for clarity.

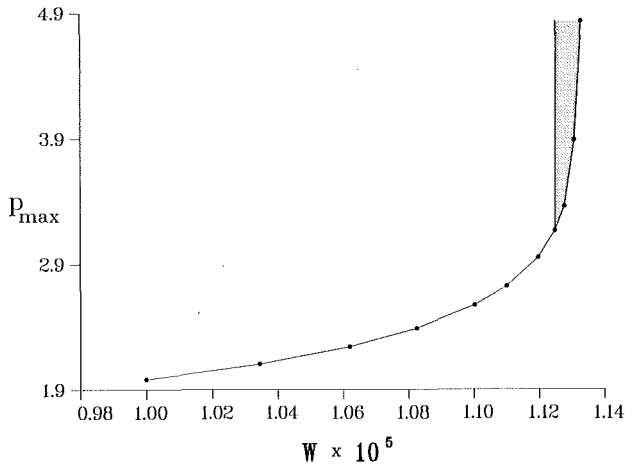

Fig. 5 Maximum pressure versus load parameter, W, for $U = 1 \times 10^{-11}$, $G = 4 \times 10^3$. As discussed in text, true curve must run through shaded area.

Results

The results presented in Figs. 1-3 are fully converged: they are insensitive to further mesh refinement. Although not generally necessary, we took the additional precaution of checking each final solution against a more refined discrete solution after halving each mesh interval. Our measure of sensitivity is that the maximum pressure value and position should not change appreciably when viewed on a length scale in which the pressure spike appears smooth (see Fig. 4).

Figure 1(*a*) shows the pressure and film thickness of a solution for a relatively large α of 10, although the difficulty in obtaining the solution was moderated by the relatively small value of .04 for λ. In this parameter regime, a relatively Hertzian pressure profile is evident with an added pressure spike. 827 nonuniform, automatically generated mesh points were used to produce this solution. Every sixth point is shown on the pressure profile in Fig. 1(*a*). Figure 1(*b*) is an expanded view of the pressure with every mesh point shown in the vicinity of the pressure maximum, and it clearly shows that the spike is indeed smooth. The largest e_j for this solution is .0060, and the ratio of maximum to minimum mesh size is 2048, the largest of the solutions reported here.

The last two solutions are part of a continuation series in which the load is increased. Using the three dimensionless parameters of Dowson and Higginson [11] (U: speed, G: material, W: load), with U and G fixed, respectively, at 1×10^{-11} and 4×10^3, Fig. 2 corresponds to $W = 1 \times 10^{-5}$ and Fig. 3 corresponds to $W = 1.125 \times 10^{-5}$. In general, the two nondimensional systems are linked by

$$\alpha = G\sqrt{W/(2\pi)}, \quad \lambda = 3\pi^2 U/W^2. \tag{21}$$

We interpret our results in terms of (U, G, W) for these particular parameters to more easily compare to the work of others. However, it is not possible in general to uniquely map from (α,λ) to the redundant (U, G, W).

The solution in Fig. 2 was generated with 518 nonuniform mesh points. It attained a maximum e_j of .0011 with a ratio of maximum to minimum mesh ratio of 64. This is the least difficult solution of those reported here.

The parameters used in Fig. 2 allow comparison with two of the more recent numerical approaches to this problem. Figure 2 of this work and Fig. 9 of Okamura [4] and Fig. 2 of Lubrecht [6] show some qualitative similarity, but poor quantitative agreeement. The pressure profile just to the left of the spike in [4] is flatter than that reported here or in [6]. Okamura places the pressure spike near $x = .5$; Lubrecht places it near $x = .2$; it is near $x = .3$ in this work. After multiplying by a factor of 2 in the two earlier papers to compensate for the difference in nondimensionalization, Okamura's results give a film thickness at the center of contact ($x = 0$) of approximately 1.6, Lubrecht gives it as approximately 2.0, it is given as 1.86 in this work. Clearly, numerical accuracy deserves more attention than it has previously received.

In Fig. 3, a continuation of the Fig. 2 solution is shown in which the load has increased by only 1/8 to $W = 1.125 \times 10^{-5}$, the pressure maximum has increased by more than 3/4, and the spike has narrowed considerably. This solution was obtained using 927 mesh points with a ratio of maximum to minimum mesh spacing of 598. The maximum e_j is .0064, surprisingly close to that of the solution in Fig. 1.

To provide a graphic example of insensitivity to further refinement, Fig. 4 shows the tip of the pressure spike for various discrete solutions that eventually produced the solution in Fig. 3. This figure illustrates our general experience that the tip of the spike rises and moves closer to the exit as the mesh is refined. Past 927 points, the curves are nearly indistinguishable, so the discrete solution is accepted.

Discussion

Our principal point is that previous solutions have not been able, or have not been executed with sufficient care, to provide adequate numerical accuracy and so have come to incorrect conclusions as to the nature of the pressure spike. The solutions given in this paper clearly show that an appropriate numerical scheme can resolve the details of the smooth pressure profile on the appropriately small length scale near the pressure maximum. The extremely nonuniform, adaptively generated meshes used to obtain these solutions show the futility of economically obtaining an accurate solution with a uniform mesh. With little assistance from the user the solutions obtained by the proposed method can be used to obtain fully converged solutions: the addition of points anywhere in the mesh will not change the solution. This feature is not present in previous work. For example, Fig. 3 of [5] and Fig. 4 of [6] show that even the most detailed previous solutions are not fully converged. During mesh refinement but before convergence has been achieved, our experience confirms that the maximum pressure of the spike increases as the mesh spacing is decreased. This behavior, observed by others, has caused some to conclude that the pressure spike is a singularity [3], or that no amount of refinement will limit the

height of the pressure spike [6]. On the other hand, Houpert and Hamrock [5] state that sufficiently many points can resolve the height of the pressure spike, and Lubrecht [6] states that smaller discretization errors are needed.

Having recognized that insufficiently refined solutions will produce smaller pressure spikes than the true solution, we must question the observation by some authors ([4-6]) that the height of the pressure spike eventually decreases with load. Their conclusion, which has been based on calculations using a fixed number of mesh points, should only be accepted if each reported solution has fully converged so that the maximum pressure has been able to achieve its full value. As shown in Fig. 4, an unconverged solution will underestimate the value of the pressure maximum. Also the narrowness of the pressure spike in the high load regime causes us to question the ability of a fixed-mesh procedure to capture even the qualitative character of the spike.

We admit that Fig. 2 and 3 only carry us to $W = 1.125 \times 10^{-5}$, a value that is not necessarily in the regime where others report the decreasing pressure spike with load. However, we have seen no sign of this decrease in our converged solutions. Figure 5 shows our experience that the maximum pressure increases very sharply with increasing load for the higher load cases. The last three points in Fig. 5 represent discrete solutions that have not fully converged (we placed an arbitrary limit of 1000 points for solutions that we would report in detail here). However, with the observation that the pressure maximum increases with refinement, we expect the true curve to actually be above that plotted in Fig. 5 and to occur somewhere in the shaded region. We believe that computational cost is the only barrier to carrying Fig. 5 accurately to higher loads using the techniques presented here.

Wu [12] has recently shown that the derivative of pressure is continuous for sufficiently small α. However, small α is the nearly isoviscous case, and Herrebrugh [7] had previously concluded that no pressure spike occurs for constant viscosity. A proof that the pressure derivative is continuous for general problems, not requiring near-constant viscosity, is still a very worthwhile goal. In the meantime, our numerical results settle this controversy in general—the pressure spike of elastohydrodynamic lubrication is smooth.

Acknowledgements

The authors would like to thank Dr. D. C. Sun of the General Motors Research Laboratories for his encouragement and technical advice, and Dr. Michael M. Kostreva of Clemson University for introducing us to this problem and for many interesting discussions while he was at our laboratories.

References

1 Hamrock, B. J., and Jacobsen, B. O., "Elastohydrodynamic Lubrication of Line Contacts," *ASLE Transactions*, Vol. 24, No. 4, 1984, pp. 275–287.

2 Kostreva, M. M., "Elasto-hydrodynamic Lubrication: A Non-Linear Complementarity Problem," *Int. J. for Numerical Methods in Fluids*, Vol. 4, 1984, pp. 377–397.

3 Kostreva, M. M., "Pressure Spikes and Stability Considerations in Elasto-hydrodynamic Lubrication-Models," ASME JOURNAL OF TRIBOLOGY, Vol. 106, 1984, pp. 386–395.

4 Okamura, H., "A Contribution to the Numerical Analysis of Isothermal Elastohydrodynamic Lubrication," *Tribology of Reciprocating Engines: Proceedings of the 9th Leeds-Lyon Symposium on Tribology*, Butterworths, Guilford, England, 1982, 313–320.

5 Houpert, L. G., and Hamrock, B. J., "Fast Approach for Calculating Film Thicknesses and Pressures in Elastohydrodynamically Lubricated Contacts at High Loads," ASME JOURNAL OF TRIBOLOGY, Vol. 108, 1985, pp. 441–420.

6 Lubrecht, A. A., ten Napel, W. E., and Bosma, R., "Multigrid, an Alternative Method for Calculating Film Thickness and Pressure Profiles in Elastohydrodynamically Lubricated Line Contacts," ASME JOURNAL OF TRIBOLOGY, Vol. 108, No. 4, 1986, pp. 551–556.

7 Herrebrugh, K., "Solving the Incompressible and Isothermal Problem in Elastohydrodynamic Lubrication Through an Integral Equation," ASME JOURNAL OF LUBRICATION TECHNOLOGY, Vol. 90, 1968, pp. 262–270.

8 Rohde, S. M., and Oh, K. P., "A Unified Treatment of Thick and Thin Film Elastohydrodynamic Problems by Using Higher Order Element Methods," *Proc. R. Soc. Lond.*, A Vol. 343, 1975, pp. 315–331.

9 Lentini, M., and Pereyra, V., "An Adaptive Finite Difference Solver for Nonlinear Two-Point Boundary Problems with Mild Boundary Layers," *SIAM Journal Numerical Analysis*, Vol. 14, No. 1, 1977, pp. 91–111.

10 Smooke, M. D., "Solution of Burner-Stabilized Premixed Laminar Flames by Boundary Value Methods," *J. Comp. Physics*, Vol. 48, 1982, pp. 72–105.

11 Dowson, D., and Higginson, G. R., "A Numerical Solution to the Elasto-Hydrodynamic Problem," *Journal Mechanical Engineering Science*, Vol. 1, No. 1, 1959, pp. 6-15.

12 Wu, S. R., "A Penalty Formulation and Numerical Approximation of the Reynolds-Hertz Problem of Elastohydrodynamic Lubrication," *International Journal Engineering Science*, Vol. 24, No. 6, 1986, pp. 1001–1013.